Nanotechnology

DOI: 10.1002/anie.201101881

Plasma-Assisted Dissociation of Organometallic Vapors for Continuous, Gas-Phase Preparation of Multimetallic Nanoparticles**

*Pin Ann Lin and R. Mohan Sankaran**

Metal nanoparticles (NPs) are characterized by novel electronic, optical, magnetic, and catalytic properties radically different from their bulk counterparts. A special class of metal NPs because of their unique multifunctional[1–3] and synergistic[4,5] properties is multimetallic NPs which are composed of two or more distinct metal elements with alloyed, core–shell, or other architectures. Despite the development of numerous synthetic routes for metal NP synthesis, the preparation of multimetallic NPs with controlled size, composition, morphology, and purity remains a significant challenge. Broadly speaking, multimetallic NPs have been synthesized by two strategies, that is, either in the liquid or gas phase. Liquid-phase methods involve the reduction of a metal salt dissolved in solution by a chemical reducing agent, such as $NaBH_4$.[6] However, when two or more metal salts are co-reduced to produce multimetallic NPs, differences in the reduction potential for the individual metal ions result in random particle compositions or morphologies.[7,8] In addition, surfactants, which are needed to control particle nucleation and growth, can adversely affect particle properties.[9] Alternatively, metal NPs have been produced in the gas phase, without chemical reducing agents or surfactants, by flame pyrolysis[10] and laser ablation.[11,12] Unfortunately, these gas-phase approaches are complex and have suffered from excessive particle growth and aggregation, making them far less useful than liquid-phase approaches for metal NP synthesis.[13] Moreover, few reports exist of multimetallic NP synthesis in the gas phase.[14–16]

Herein, we present a plasma-based scheme for the preparation of multimetallic NPs. Nanoparticles are synthesized from vapors of organometallic compounds such as bis(cyclopentadienyl)nickel $[Ni(Cp)_2]$[17] or copper acetylacetonate $[Cu(acac)_2]$[18] that have a long history in metal–organic chemical vapor deposition (MOCVD) of thin films. In our process, these same MOCVD precursors are dissociated in a plasma to homogeneously nucleate particles in the gas phase. The combination of a microreactor geometry,[19,20] characterized by extremely short residence times of approximately 1 millisecond, and a plasma environment[21–23] which charges the particles, yields narrow size distributions of nanometer-sized particles (less than 5 nm in diameter) in a single step. By carefully combining precursor vapors, we demonstrate that a wide range of size and compositionally controlled multimetallic NPs can be produced by this approach.

Multimetallic metal NPs were synthesized by introducing vapors of various organometallic compounds into a direct current (dc), atmospheric-pressure microplasma reactor (Figure 1)[24,25] There are many of these type of precursors available; we have chosen four to demonstrate the methodology: bis(cyclopentadienyl)iron $[Fe(Cp)_2]$, $[Ni(Cp)_2]$, $[Cu(acac)_2]$, and platinum acetylacetonate $[Pt(acac)_2]$. We initially studied the nucleation and growth of pure metal NPs by aerosol size classification. We note that the aerosol instrument has a detection limit of 2.0 nm; smaller particles are produced in the plasma, but must be characterized by other techniques such as TEM. Nonetheless, the aerosol instrument is a valuable in situ diagnostic, particularly for multimetallic NPs as will be discussed later. Figure 2a and b show particle size distributions (PSDs) for Ni and Cu NPs synthesized from the respective metal precursors at various precursor flow rates. The PSDs were fit to a log-normal distribution[26] to obtain the geometric mean particle diameter (D_{pg}) and

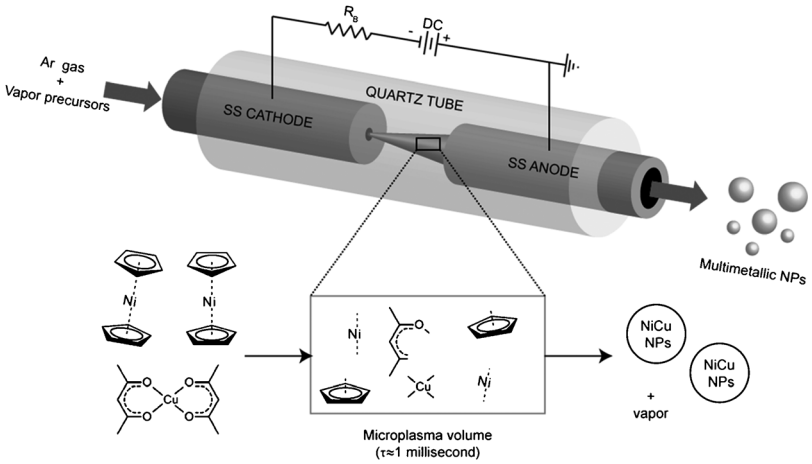

Figure 1. Schematic diagram of direct-current (dc), atmospheric-pressure microplasma reactor used to dissociate organometallic vapors and continuously synthesize multimetallic nanoparticles (NPs). A hypothesized mechanism for formation of NiCu bimetallic NPs is also shown. Vapor precursors are dissociated in the plasma volume (τ is the residence time) to form radical moieties that nucleate multimetallic NPs.

[*] P. A. Lin, Prof. R. M. Sankaran
Department of Chemical Engineering
Case Western Reserve University
10900 Euclid Avenue, Cleveland, OH 44106-7217 (USA)
E-mail: mohan@case.edu

[**] We acknowledge funding from the NSF CAREER Award Program (CBET-0746821). R.M.S. also thanks the AFOSR Young Investigator Program and the Camille Dreyfus Teacher-Scholar Awards Program for their support.

Supporting information for this article is available on the WWW under http://dx.doi.org/10.1002/anie.201101881.

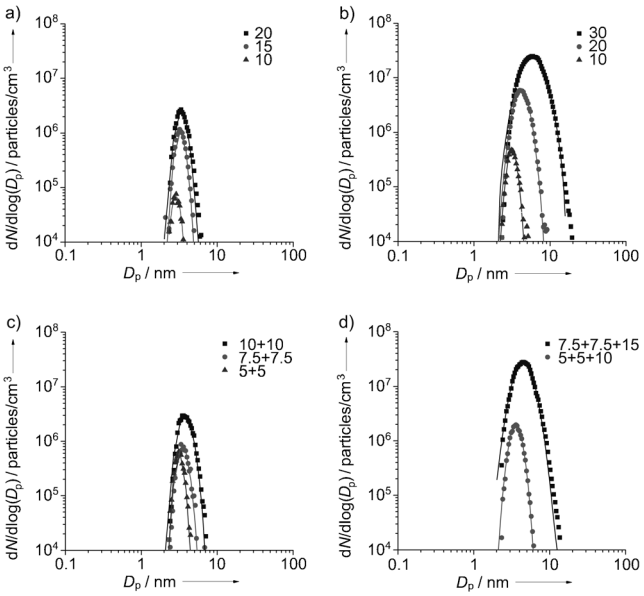

Figure 2. Particle size distributions (PSDs) obtained by aerosol size classification for as-grown a) Ni, b) Cu, c) $Ni_{0.47}Cu_{0.53}$, and d) $Ni_{0.22}Fe_{0.29}Cu_{0.49}$ NPs synthesized in the plasma reactor from their respective metal precursors at the indicated precursor flow rates (sccm). For example, in (d), 7.5 + 7.5 + 15 represents 7.5 sccm of the Ni and Fe precursors, respectively, and 15 sccm of the Cu precursor. In all cases, the metal precursor flow was diluted with a flow of pure Ar gas and the total flow rate through the plasma reactor was 100 sccm. D_p = particle diameter; N = number of particles.

geometric standard deviation (σ_g). In addition to Ni and Cu, we also synthesized Fe and Pt NPs (see Supporting Information). For all metal precursors, D_{pg}, σ_g, and the particle number concentration were observed to increase with precursor flow rate. Assuming that particle nucleation/growth is a first order process, a higher precursor flow rate results in more particles being nucleated and increases the growth rate (by vapor deposition). Thus, the mean diameter and the particle concentration both increase, the increasing particle concentration of which leads to particle agglomeration.

To synthesize multimetallic NPs, the precursors were combined at different flow rates. Although the mechanism for particle nucleation and growth may be very complicated and depend on the precursor vapor concentration, enthalpy of dissociation (ΔH_d) of the individual precursors, and other plasma parameters, we infer that aerosol measurements can be used to predict the size and composition of our multimetallic NPs. For example, the expected composition of Ni_xCu_{1-x} NPs (where x is the estimated atomic fraction of Ni) was calculated from the following empirical equation [Eq (1)]

$$x = \frac{F_{Ni} D_{pg,Ni\,NPs}}{F_{Ni} D_{pg,Ni\,NPs} + F_{Cu} D_{pg,Cu\,NPs}} \quad (1)$$

where F is the precursor flow rate and D_{pg} is the mean particle diameter of the pure metal NPs obtained from aerosol measurements. This analysis is based on a linear relationship between particle diameter and precursor flow rate and an overall assumption that all precursors form particles similarly (see Supporting Information). Using Equation (1), we estimate that at equal flow rates of the Ni and Cu precursor, the composition of the bimetallic NPs is 47% Ni and 53% Cu (i.e. $Ni_{0.47}Cu_{0.53}$). The mean diameter was then varied (at constant composition) by changing the total precursor flow rate in Ar, analogous to the pure metal NPs (Figure 2c). This approach can be extended to other bimetallic NPs and trimetallic NPs. In Figure 2d, PSDs are shown for $Ni_{0.22}Fe_{0.29}Cu_{0.49}$ NPs synthesized with mean diameters from 3.7 to 4.8 nm. All of our aerosol results are summarized in Table 1.

The multimetallic NPs were also evaluated by ex situ materials characterization. TEM images of as-grown Cu, $Ni_{0.78}Cu_{0.22}$, $Ni_{0.47}Cu_{0.53}$, and $Ni_{0.22}Fe_{0.29}Cu_{0.49}$ NPs are shown in Figure 3a–d. The images reveal that the particles are uniform, spherical, and unagglomerated. Histograms of the particle diameters were obtained from the TEM images and agree well with aerosol results (Supporting Information, Figure 2S). The high-resolution images in Figure 3e and f of a representative $Ni_{0.47}Cu_{0.53}$ and $Ni_{0.22}Fe_{0.29}Cu_{0.49}$ NP, respectively, show that the particles are crystalline. The measured lattice spacings of 0.20 nm and 0.21 nm, respectively, are qualitatively consistent with the incorporation of the different metals in the respective NP lattices since bulk Ni(111) and Cu(111) lattices exhibit spacings of 0.203 and 0.204 nm, respectively. These results suggest that organic moieties from the precursor are not incorporated in the cores of the particle; however, we cannot completely rule out the presence of carbon in the as-grown material since the TEM grids themselves consist of carbon films. To more carefully analyze the formation of carbon from the precursors, we performed X-ray photoelectron spectroscopy (XPS) on films of NPs deposited from the gas phase onto Si substrates (see Supporting Information).

Table 1: Summary of aerosol measurements for mono-, bi-, and trimetallic NPs synthesized in the plasma reactor from various organometallic compounds.

NP	Metal precursor	Vapor pressure	Metal precursor flow rate [sccm]	D_{pg} [nm]	σ_g
Ni	$[Ni(Cp)_2]$	13 torr (293 K)[a]	20	3.5	1.15
			15	3.3	1.13
			10	2.8	1.07
Fe	$[Fe(Cp)_2]$	15 torr (293 K)[a]	20	4.7	1.22
			15	4.2	1.19
			10	3.8	1.16
Cu	$[Cu(acac)_2]$	14 torr (383 K)[b]	30	5.9	1.30
			20	3.9	1.19
			10	3.2	1.12
Pt	$[Pt(acac)_2]$	500 torr (455 K)[c]	20	3.5	1.19
			10	2.7	1.09
$Ni_{0.47}Cu_{0.53}$			10 + 10	3.9	1.18
			7.5 + 7.5	3.6	1.15
			5 + 5	3.2	1.12
$Ni_{0.18}Cu_{0.82}$			5 + 20	5.3	1.30
			4 + 16	4.5	1.25
$Ni_{0.22}Fe_{0.29}Cu_{0.49}$			7.5 + 7.5 + 15	4.8	1.25
			5 + 5 + 10	3.7	1.16
$Ni_{0.34}Fe_{0.46}Cu_{0.20}$			10 + 10 + 5	4.5	1.21

[a] Ni and Fe precursors were sublimed at room temperature. [b] Cu precursor was sublimed at 383 K. [c] Pt precursor was sublimed at 373 K.

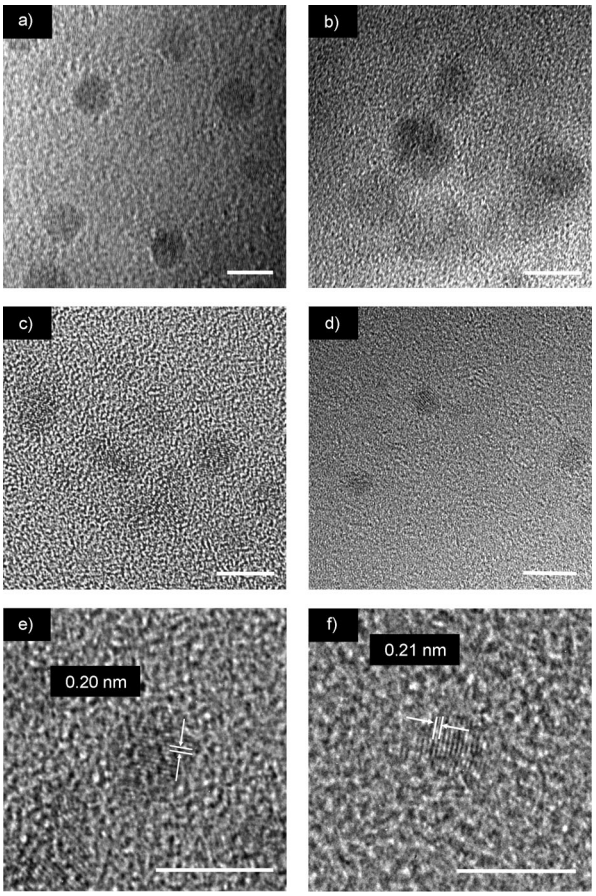

Figure 3. TEM images of as-grown a) Cu, b) $Ni_{0.78}Cu_{0.22}$, c) $Ni_{0.47}Cu_{0.53}$, and d) $Ni_{0.22}Fe_{0.29}Cu_{0.49}$ NPs. High-resolution images of a representative e) $Ni_{0.47}Cu_{0.53}$ and f) $Ni_{0.22}Fe_{0.29}Cu_{0.49}$ NP are also shown that have lattice spacings of 0.20 and 0.21 nm, respectively. All scale bars are 5 nm.

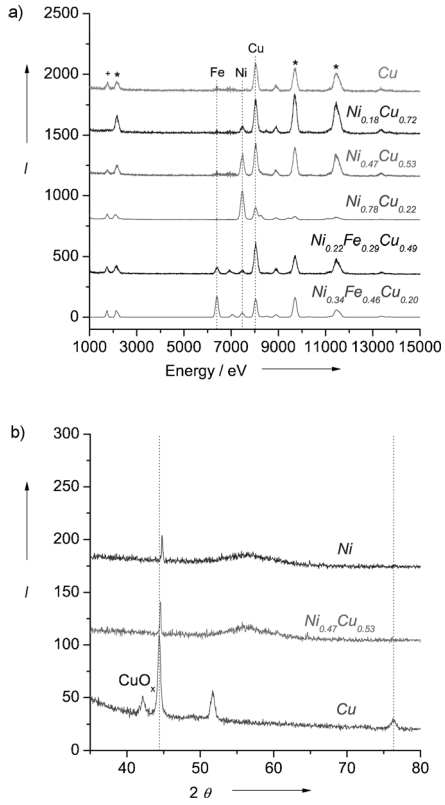

Figure 4. a) Energy dispersive X-ray (EDX) spectra of various compositions of Ni_xCu_{1-x} and $Ni_xFe_yCu_{1-x-y}$ NPs. The NiK_α, CuK_α, and FeK_α lines are indicated, as well as lines corresponding to Au (*) from the TEM substrate and Si (+) from the EDX detector. b) X-ray diffraction (XRD) patterns of Ni, Cu, and Ni_xCu_{1-x} NPs. A dotted line corresponding to the position of the (111) diffraction peak for fcc Cu is included as a guide. A peak ascribed to copper oxide (CuO_x) is also indicated.

Our XPS data indicates that a negligible amount of carbon is present in the as-grown material. Figure 4a shows a series of EDX spectra obtained for Ni_xCu_{1-x} and $Ni_xFe_yCu_{1-x-y}$ NPs of varying composition. We find that the intensity of the spectral lines corresponding to the various metals change as expected for the different particle compositions. XRD spectra of Ni_xCu_{1-x} NPs ($D_{pg} \approx 4.0$ nm) are shown in Figure 4b. A diffraction peak at 44.81° corresponding to the (111) crystalline plane of face-centered cubic (fcc) Ni, and at 44.32, 51.64 and 76.24° corresponding to the (111), (200) and (220) crystalline planes, respectively, of fcc Cu, were observed for the pure Ni and Cu NPs, respectively. The XRD pattern for $Ni_{0.47}Cu_{0.53}$ shows a small shift of the Ni and Cu (111) diffraction peaks, indicating that the bimetallic NPs are alloys which is consistent with TEM observations.

We compared the ratio of the NiK_α and CuK_α lines in the EDX spectra to the Cu atomic fraction predicted by Equation (1) for our Ni_xCu_{1-x} NPs (Figure 5). The actual composition of Ni and Cu in $Ni_{0.78}Cu_{0.22}$, $Ni_{0.47}Cu_{0.53}$, and $Ni_{0.18}Cu_{0.82}$ NPs was determined to be 0.73:0.27, 0.40:0.60, and 0.10:0.90, respectively from the EDX spectra. The composition of $Ni_{0.47}Cu_{0.53}$ NPs was independently ascertained from the XRD data to be 0.46:0.54 by applying Vegard's Law which assumes that the lattice constant of an alloy depends linearly on the lattice constants of the individual metal components. From Figure 5, it is apparent that XRD analysis shows excellent correspondence with aerosol measurements, whereas EDX analysis overestimates the Cu content. Sepa-

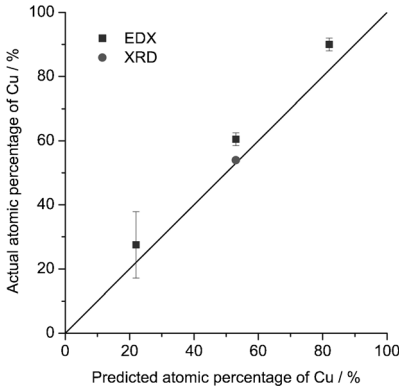

Figure 5. Comparison of actual Cu atomic composition, as independently determined by EDX and XRD analysis, and predicted Cu atomic composition, as estimated by our empirical expression [Eq. (1)], for Ni_xCu_{1-x} NPs. The EDX data points, along with error bars, represent an average of at least 5 spectra obtained across each sample area. The line is included as a guide.

rately, the compositions of our trimetallic NPs were determined by EDX to be 0.13:0.19:0.68 and 0.15:0.36:0.49 for $Ni_{0.22}Fe_{0.29}Cu_{0.49}$ and $Ni_{0.34}Fe_{0.46}Cu_{0.20}$, respectively (see Supporting Information). EDX characterization has been previously reported to be less accurate in estimating metal content.[27] Nonetheless, the results show that the composition of the multimetallic NPs can be tuned and, within some error, have the expected atomic fraction of the individual metals.

In summary, a gas-phase approach for the synthesis of multimetallic NPs by plasma-assisted dissociation of organometallic vapors has been presented. The atomic-scale composition of the NPs is tunable, independent of size, by varying the flow rates (i.e. vapor concentrations) of the different metal precursors. The process is potentially scalable, by operating large arrays of microplasmas in parallel, low cost, and high purity, as it does not use surfactants to control particle nucleation and growth. Moreover, the method is generic, since there are many of these types of MOCVD precursors available, and should allow preparation of a wide range of multimetallic NPs for applications as novel multifunctional materials.

Experimental Section

Bis(cyclopentadienyl)nickel [$Ni(Cp)_2$] (Sigma Aldrich), bis(cyclopentadienyl)iron [$Fe(Cp)_2$] (Fisher Scientific), copper acetylacetonate [$Cu(acac)_2$] (Sigma Aldrich), and platinum acetylacetonate [$Pt(acac)_2$] (Fisher Scientific) were used as metal precursors. In general, the precursors were introduced into the plasma reactor from separate gas lines by subliming a solid powder, sealed inside a stainless steel tube, with a flow of Ar gas and diluting with an additional flow of pure Ar. Both [$Ni(Cp)_2$] and [$Fe(Cp)_2$] were sublimed at room temperature while [$Cu(acac)_2$] and [$Pt(acac)_2$] were sublimed at 383 and 373 K, respectively. To prevent condensation, the gas lines downstream of the metal precursors were held at 453 K which is lower than the decomposition temperatures of any of the precursors. Digital mass flow controllers were used to control all gas flow rates. The total gas flow rate in the plasma reactor was 100 sccm in all experiments.

In situ aerosol size classification was performed with a scanning mobility particle sizing (SMPS) system (Model 3936, TSI. Inc.). The as-grown particles exiting the plasma reactor were diluted with N_2 (1.4 slm) to avoid excessive particle agglomeration and immediately introduced into the aerosol instrument to obtain particle size distributions (PSDs)

Ex situ particle characterization was carried out by depositing the NPs directly from the gas phase onto substrates by electrostatic precipitation (Model 3089, TSI, Inc.). TEM samples were made by depositing for 1 h on carbon-coated Au grids. HRTEM was performed using a Philips Tecnai F30 field-emission high-resolution transmission electron microscope operated at 300 kV. The atomic composition of the multimetallic NPs was verified by EDX with a convergent beam and a Li-drifted Si detector with 130 eV energy resolution. XRD and XPS samples were made by depositing NPs onto Si wafers. XRD characterization was performed with a Scintag X-1 advanced X-ray diffractometer using monochromated CuK_α radiation ($\lambda = 0.1542$ nm). XPS measurements were carried out with a PHI VersaProbe XPS Microprobe. A monochromatic Al K_α X-ray (1486.6 eV) source was used with a spot size of 300 μm.

Received: March 16, 2011
Revised: June 29, 2011
Published online: September 22, 2011

Keywords: chemical vapor deposition · copper · microplasma · nanoparticles · nickel

[1] J. L. Lyon, D. A. Fleming, M. B. Stone, P. Schiffer, M. E. Williams, *Nano Lett.* **2004**, *4*, 719 – 723.
[2] X. Gao, L. Yu, R. I. MacCuspie, H. Matsui, *Adv. Mater.* **2005**, *17*, 426 – 429.
[3] C. Wang, D. Vliet, K. L. More, N. J. Zaluzec, S. Peng, S. Sun, H. Daimon, G. Wang, J. Greeley, J. Pearson, A. P. Paulikas, G. Karapetrov, D. Strmcnik, N. M. Markovic, V. R. Stamenkovic, *Nano Lett.* **2011**, *11*, 919 – 926.
[4] J. Y. Park, Y. Zhang, M. Grass, T. Zhang, G. A. Somorjai, *Nano Lett.* **2008**, *8*, 673 – 677.
[5] W.-H. Chiang, R. M. Sankaran, *Adv. Mater.* **2008**, *20*, 4857 – 4861.
[6] G. Frens et al., *Nature Phys. Sci.* **1973**, *241*, 20 – 22.
[7] I. Srnová-Šloufová, B. Vlčková, Z. Bastl, T. L. Hasslett, *Langmuir* **2004**, *20*, 3407 – 3415.
[8] F. Tao, M. E. Grass, Y. W. Zhang, D. R. Butcher, J. R. Renzas, Z. Liu, J. Y. Chung, B. S. Mun, M. Salmeron, G. A. Somorjai, *Science* **2008**, *322*, 932 – 934.
[9] Z. Liu, C. Yu, I. A. Rusakova, D. Huang, P. Strasser, *Top. Catal.* **2008**, *49*, 241 – 250.
[10] H. K. Kammler, L. Mädler, S. E. Pratsinis, *Chem. Eng. Technol.* **2001**, *24*, 583 – 596.
[11] M. Ullmann, S. K. Friedlander, A. Schmidt-Ott, *J. Nanopart. Res.* **2002**, *4*, 499 – 509.
[12] S. Eliezer, N. Eliaz, E. Grossman, D. Fisher, I. Gouzman, Z. Henis, S. Pecker, Y. Horovitz, M. Fraenkel, S. Maman, Y. Lereah, *Phys. Rev. B* **2004**, *69*, 144119.
[13] D. Wang, Y. Li, *Adv. Mater.* **2011**, *23*, 1044 – 1060.
[14] H. Lillich, J. Wolfrum, V. Zumbach, L. E. Aleandri, D. J. Jones, J. Rozihre, P. Albers, K. Seibold, A. Freund, *J. Phys. Chem.* **1995**, *99*, 12413 – 12421.
[15] R. Strobel, J-D. Grunwaldt, A. Camenzind, S. E. Pratsinis, A. Baiker, *Catal. Lett.* **2005**, *104*, 9 – 16.
[16] S. Senkan, M. Kahn, S. Duan, A. Ly, C. Leidhom, *Catal. Today* **2006**, *117*, 291 – 296.
[17] G. J. M. Dormans, *J. Cryst. Growth* **1991**, *108*, 806 – 816.
[18] J. Pelletier, R. Pantel, J. C. Oberlin, Y. Pauleau, P. Gouy-pailler, *J. Appl. Phys.* **1991**, *70*, 3862 – 3866.
[19] J. B. Edel, R. Fortt, J. C. deMello, A. J. deMello, *Chem. Commun.* **2002**, 1136 – 1137.
[20] K. H. Brian, K. F. Jensen, M. G. Bawendi, *Angew. Chem.* **2005**, *117*, 5583 – 5587; *Angew. Chem. Int. Ed.* **2005**, *44*, 5447 – 5451.
[21] J. P. Borra, *J. Phys. D* **2006**, *39*, R19 – R54.
[22] A. Bapat, C. R. Perrey, S. A. Campbell, C. B. Carter, U. Kortshagen, *J. Appl. Phys.* **2003**, *94*, 1969 – 1974.
[23] U. Kortshagen, U. Bhandarkar, *Phys. Rev. E* **1999**, *60*, 887.
[24] R. M. Sankaran, K. P. Giapis, *J. Appl. Phys.* **2002**, *92*, 2406.
[25] D. Mariotti, R. M. Sankaran, *J. Phys. D* **2010**, *43*, 323001.
[26] J. H. Seinfeld, S. N. Pandis, *Atmospheric Chemistry and Physics*, Wiley, New York, NY, **1998**.
[27] N. E. Motl, E. Ewusi-Annan, I. T. Sines, L. Jensen, R. E. Schaak, *J. Phys. Chem. C* **2010**, *114*, 19263 – 19269.

